Soft Matter

RSC Publishing

PAPER

View Article Online
View Journal

Secondary structure and rigidity in model proteins†

Cite this: DOI: 10.1039/c3sm50807b

Stefania Perticaroli,‡§[ab] Jonathan D. Nickels,‡§[ac] Georg Ehlers,‡[d] Hugh O'Neill,‡[ef] Qui Zhang‡[ef] and Alexei P. Sokolov‡*[abc]

Received 20th March 2013
Accepted 8th August 2013

DOI: 10.1039/c3sm50807b

www.rsc.org/softmatter

There is tremendous interest in understanding the role that secondary structure plays in the rigidity and dynamics of proteins. In this work we analyze nanomechanical properties of proteins chosen to represent different secondary structures: α-helices (myoglobin and bovine serum albumin), β-barrels (green fluorescent protein), and α + β + loop structures (lysozyme). Our experimental results show that in these model proteins, the β motif is a stiffer structural unit than the α-helix in both dry and hydrated states. This difference appears not only in the rigidity of the protein, but also in the amplitude of fast picosecond fluctuations. Moreover, we show that for these examples the secondary structure correlates with the temperature- and hydration-induced changes in the protein dynamics and rigidity. Analysis also suggests a connection between the length of the secondary structure (α-helices) and the low-frequency vibrational mode, the so-called boson peak. The presented results suggest an intimate connection of dynamics and rigidity with the protein secondary structure.

Introduction

Proteins are hierarchically organized biomolecules, with the primary amino acid sequence arranged in characteristic secondary structures, such as α-helices, β-strands, turns and loops. These in turn are folded and assembled to assume a characteristic three-dimensional structure that is closely related to the protein's function, dynamics, and mechanical properties.[1,2] Understanding the intrinsic rigidity of single structural components of proteins, such as α-helices or β-sheets, is crucial to disentangling the relationships between structure, mechanical properties, dynamics, and function in biological systems.

There are numerous examples of elastic properties casually assigned to secondary structure, such as the α-helix motif, which is widely found in the cytoskeleton, hair, hooves and wool.[3] It is also the protein structural element that most commonly crosses biological membranes[4] and plays a fundamental role in imparting mechanical stability to cells. α-Helix proteins also participate in processes involving mechanical signalling[5] and signal transduction.[6] Collagen is a related example. Thanks to its tough and robust fibrous structure made of arrays of triple left-handed helices, collagen is able to easily dissipate large elastic energy during deformation and is characterized by a global mechanical stiffness, as measured by a Young's (or elastic) modulus (E) of 1.5–10 GPa.[7] Proteins containing a large content of the β-sheet motif also show remarkable mechanical properties.[7–9] The β-sheet motif is the predominant secondary structure in muscle tissue,[3] amyloids and beta-solenoid protein nanotubes,[10] silk[11,12] and insulin amyloid fibrils.[13] Spider and silkworm silk can be composed of more than 50% β-sheets.[11] Insulin amyloid fibrils and spider silk, hierarchical architectures of highly organized and densely packed H-bonded β-sheets,[12,13] have been shown to have Young's moduli of 3.3 GPa,[13] and 1–40 GPa,[7,14] respectively, at room temperature, approaching that of many engineered inorganic materials.[7]

However, the mechanical rigidity of native protein molecules has not been systematically investigated as a function of the secondary structure. In fact, quantitative results are limited to a few single-molecule techniques such as atomic force microscopy (AFM)[15,16] and molecular dynamics (MD) simulations[2,15,17] that have focused on model systems such as single domain fibrils or amyloids, probing the mechanical response under external stress

[a]Chemical and Materials Sciences Division at Oak Ridge National Laboratory, Oak Ridge, TN, 37831, USA. E-mail: spertica@utk.edu; jnickel1@utk.edu; sokolov@utk.edu

[b]Department of Chemistry, University of Tennessee, Knoxville, TN, 37996-1600, USA

[c]Joint Institute for Neutron Sciences, Oak Ridge National Laboratory, Oak Ridge, TN, 37831, USA

[d]Quantum Condensed Matter Division, Oak Ridge National Laboratory, PO Box 2008, Oak Ridge, TN, 37831, USA. E-mail: ehlersg@ornl.gov

[e]Department of Biochemistry and Cellular and Molecular Biology, University of Tennessee, Knoxville, TN, 37996, USA

[f]Biology and Soft Matter Division, Oak Ridge National Laboratory, PO Box 2008, Oak Ridge, TN, 37831, USA. E-mail: oneilhm@ornl.gov; zhangq@ornl.gov

† Electronic supplementary information (ESI) available: Parameters used in calculations, refractive index measurements and literature values for density, longitudinal sound velocity c_L, and Young's modulus E. See DOI: 10.1039/c3sm50807b

‡ J. D. N. and S. P. designed and participated in all experiments, analyzed the data and together with A. P. S. wrote the paper; G. E. is the instrument responsible scientist at CNCS and performed and supervised the neutron scattering measurements, H. O'N. and Q. Z. produced the GFP samples.

§ S. P. and J. D. N. contributed equally to this paper.

conditions. It is difficult to generalize these findings to native proteins due to restrictions in the geometry of the molecular attachment and the necessity of limiting surface effects or interactions between individual structures.[16] In these studies mechanical properties have usually been probed at room temperature and along only one axis.[18] Moreover, such pulling experiments intrinsically change the underlying energy landscape, meaning that measured elasticity values may not accurately reflect the native state. The results of these studies raise an interesting question: if the energy of H-bonds is comparable for both α- and β-structures, why do β-sheets have such strong resistance against rupture, reaching the strength of covalent bonds, and exceeding that of α-helices by an order of magnitude?[18]

Here we present experimental studies based on light and neutron scattering spectroscopy that quantify the stiffness of proteins with different secondary structures in their native states. We analysed four proteins: myoglobin (MYO), bovine serum albumin (BSA), lysozyme (LYS) and green fluorescent protein (GFP), chosen to represent particular protein secondary structures. The first two systems are α-proteins, with BSA ($M_w \sim$ 62.6 kDa) being almost 4 times larger than myoglobin ($M_w \sim$ 17.8 kDa). GFP ($M_w \sim$ 25.8 kDa) is an 11-stranded β-barrel, and lysozyme ($M_w \sim$ 14.3 kDa) is a globular protein containing both α and β domains as well as a significant fraction of turns and loops (Table 1). Brillouin, depolarized light, and neutron scattering experiments were carried out in a wide temperature range (100–298 K) on dry and hydrated proteins. Our analysis reveals higher rigidity of GFP (protein containing β-structures) in both dry and hydrated states. This difference appears not only in a higher elastic modulus (Fig. 1), but also in more depressed dynamics on the picosecond time scale (inset Fig. 1), and in a higher frequency of the collective vibrations, the so-called boson peak. In addition, the presented analysis suggests a connection between the length scale of the secondary structure and the frequency of the boson peak in proteins.

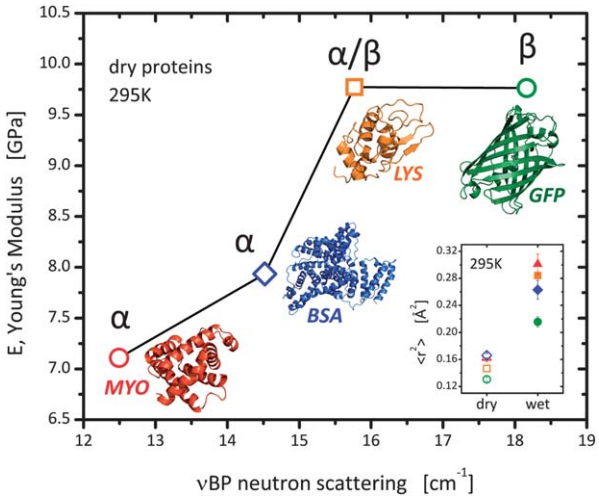

Fig. 1 The elastic modulus for the four dry proteins studied *versus* the boson peak frequency (ν_{BP}) at 295 K. In both cases, the α-proteins appear to be less rigid than those containing β-structures. Inset: atomic mean squared displacement ($\langle r^2 \rangle$) for dry and hydrated proteins at $T = 295$ K as estimated by neutron scattering. GFP exhibits the smallest $\langle r^2 \rangle$.

Materials and methods

Samples

Lysozyme from chicken egg white, bovine serum albumin and myoglobin from equine heart were purchased from Sigma-Aldrich. GFP was provided by the Bio-deuteration Lab of Oak Ridge National Laboratory.[19] All the proteins were dialyzed and lyophilized before use. The hydration level of $h \sim 0.4$ (h = grams of water/grams of protein) was obtained through isopiestic equilibration of the powder with water vapour in a closed chamber. For refractive index, Brillouin, and depolarized light scattering measurements the solvent used was H_2O, whereas D_2O was used for the neutron scattering experiments.

Table 1 Relative content of each secondary structure in the model proteins studied, as defined by mass fraction. This information has been extracted from the pdb files of the proteins (1GFL; 1LYZ; 3V03; 1DWT)

	Alpha	Beta	Loop and turn
GFP	12%	53%	35%
LYS	37%	5%	58%
BSA	77%	0%	22%
MYO	80%	0%	20%

Refractive index

The refractive indexes of all the samples were measured using a Bausch and Lomb Abbe-3L refractometer (sodium lamp, $\lambda =$ 589 nm) at 25 °C (see Table S1 in ESI†). Typical uncertainties are of the order of ~5%.

Brillouin

Polarized Brillouin spectra (Fig. 2) were measured using a Sandercock tandem Fabry–Pérot interferometer in back-scattering geometry with a solid state laser (Coherent Verdi-2) and a wavelength of 532 nm. A $d = 4$ mm mirror separation (free spectral range 37.5 GHz) and a 30 mW incident power on the sample were used. The samples (pellets of ~17–20 mg weight, ~5 mm diameter and ~0.7 mm thickness) were sealed between two sapphire windows, placed in an optical cryostat (Oxford instrument 9146) and equilibrated for at least 30 minutes at each temperature before measurements. All spectra where collected for 1–2 hours, going from the highest (298 K) to the lowest temperature (100 K).

The Brillouin spectra were fitted to the damped harmonic oscillator model

$$I(v) = A\frac{\Gamma_L \Omega_L}{\left(v^2 - \Omega_L{}^2\right)^2 + (\Gamma_L v)^2} + y_0 \quad (1)$$

where Ω_L is the frequency and Γ_L is the width of the longitudinal modes, and A and y_0 are free parameters. At each temperature both the energy loss and the energy gain peaks were fitted and their parameters averaged.[20]

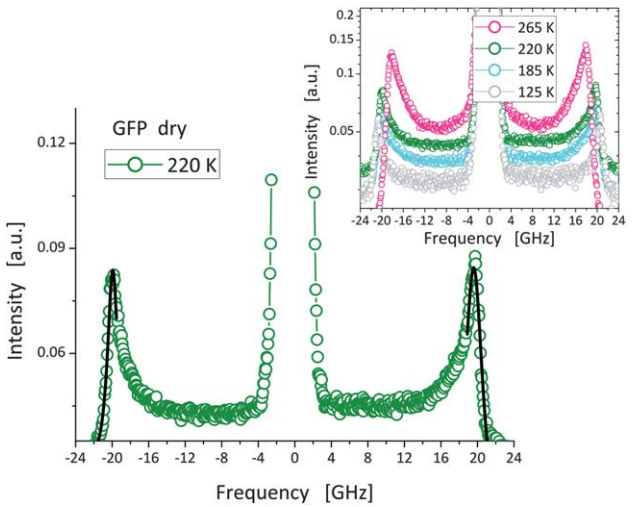

Fig. 2 Representative Brillouin spectrum of dry GFP (symbols) and the fit using eqn (1) (solid lines). Inset: Brillouin spectra for dry GFP at four different temperatures.

Depolarized light scattering and neutron scattering

Depolarized light scattering spectra (Fig. 3a) were measured in a backscattering geometry with a Jobin-Yvon T64000 triple monochromator in the frequency range $\nu \sim 8$–$520\ \mathrm{cm}^{-1}$ and with a resolution of $\sim 0.5\ \mathrm{cm}^{-1}$. A Lexel-95 Krypton-ion laser with a wavelength of 647.1 nm and 10–20 mW incident power on the sample was used as an excitation source. Depolarized light scattering measurements were performed between 170 and 298 K on samples prepared in the same fashion as the Brillouin measurements.

To verify the reproducibility of the data, measurements at the initial temperatures were repeated after the lowest temperature was reached. No detectable differences were noticed in the spectra, confirming also that the hydration level wasn't changed during the experiment. Further confirmation of the absence of loss of mass has been made by weighing the sealed sample cell at the beginning and at the end of the measurements. Strong fluorescence prevented the depolarized light scattering measurements in hydrated myoglobin. We were able to measure only the depolarized light scattering of dry myoglobin at high temperature, using the green laser (532 nm) to minimize the fluorescence contribution.

The neutron scattering experiments were carried out in the Cold Neutron Chopper Spectrometer (CNCS) at the Spallation Neutron Source (SNS)[21] with an incident energy of 3 meV and an elastic resolution of $\sim$50 μeV ($\sim$20 ps). The experimental setup provided access to a Q range from 0.2 to 4 $\mathrm{Å}^{-1}$ and a wide energy range up to $\sim$20 meV ($\sim$0.05 ps). All exchangeable hydrogen atoms in the proteins were exchanged to deuterium by dissolving the proteins in 99.9% D_2O at 10 mg ml^{-1}, for $\sim$8 hours at 4 °C, and then lyophilizing and repeating this process twice. Measurements were performed on dry samples and on protein–D_2O samples at 295 and 170 K for LYS, BSA and MYO samples and at 5 different temperatures for the GFP (295, 280, 250, 220, 170 K). 100–200 mg of protein samples (dry weight) were used in order to achieve transmission higher than 90% and avoid significant multiple scattering contribution. Further details of measurements, sample preparation and data treatment concerning the mean squared displacements of the GFP samples can be found in ref. 22.

Both depolarized light scattering and neutron scattering spectra are presented as spectral density I_n (Fig. 3). Analysed neutron scattering data correspond to the energy gain side of the spectra, therefore the spectral density has been calculated as

$$I_n^{NS} = \frac{I(\nu)}{\nu n_B(\nu)}, \tag{2}$$

where $I(\nu)$ is the measured intensity and

$$n_B(\nu) = [\exp(h\nu/kT) - 1]^{-1}, \tag{3}$$

is the Bose–Einstein occupation number.[23] Depolarized light scattering spectra were measured in the energy loss side, and consequently the spectral density was calculated by[24]

$$I_n^{LS} = \frac{I(\nu)}{\nu[n_B(\nu) + 1]}. \tag{4}$$

To estimate the boson peak frequency ν_{BP} the light and neutron scattering spectra were fitted to the following expression:[20]

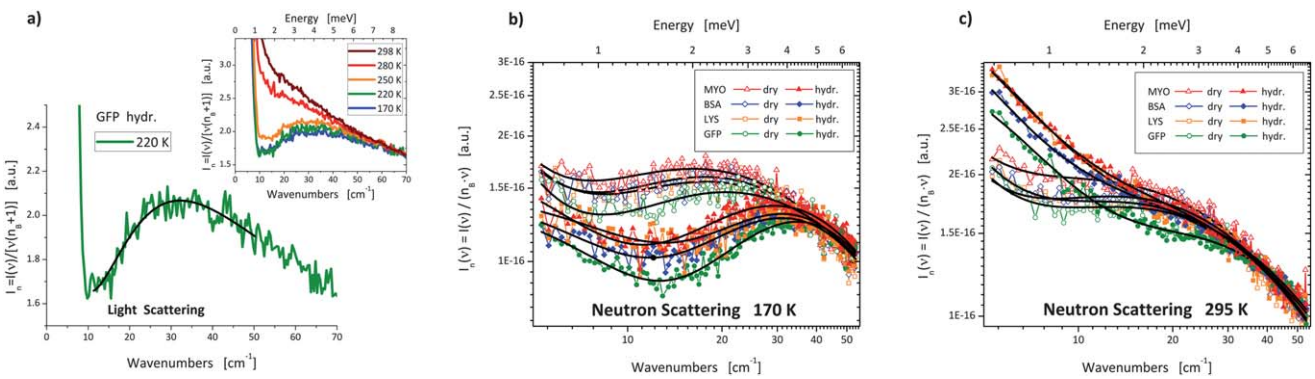

Fig. 3 (a) Depolarized light scattering spectra of the boson peak region for hydrated GFP presented as the spectral density; the black line represents the fit using eqn (5). Neutron scattering spectra in the boson peak region presented as the spectral density for dry (empty symbols) and hydrated (closed symbols) proteins at 170 K (b) and 295 K (c). The spectra have been normalized at the high frequency tail; the solid lines represent the fit using eqn (5).

$$I_n(v) = \frac{A}{v^2 + {v_0}^2} + B\exp\left[-\frac{\left(\ln \frac{v}{v_{BP}}\right)^2}{2W^2} \right] + y_0, \quad (5)$$

where the first term represents the quasielastic scattering component approximated by a Lorentzian function with the width v_0 and amplitude A, and the second term describes the boson peak in terms of a lognormal function of width W and amplitude B. In the case of neutron scattering data the parameter $y_0 = 0$.

The relative atomic mean squared displacements, $\langle r^2 \rangle$, were extracted from the elastic intensity of the neutron scattering experiment according to the standard Gaussian approximation method:[25]

$$\frac{I^{NS}(Q,T)}{I^{NS}(Q,T=0)} = e^{-\frac{1}{6}\langle r^2 \rangle Q^2}. \quad (6)$$

The elastic intensity, $I_{el}(Q)$, was defined as the integrated intensity ± 30 μeV from the central line (~10 ps).[21] $\langle r^2 \rangle$ was then extracted by fit of the plot of the natural logarithm of the normalized intensity *versus* Q^2 over a Q range of 0.5 to 2.1 Å^{-1}. In this study we use 170 K as the low temperature reference.

Results and discussion

Brillouin scattering is the inelastic scattering of light by elastic sound waves propagating in a medium.[26,27] The Brillouin spectra of transparent powders exhibit a characteristic broad band with a high-frequency cut-off (Fig. 2). These spectra represent the scattering at various angles between 0 and 180 degrees,[28] caused by multiple reflections and refractions.[20,28] It has been demonstrated that the cut-off frequency Ω_L corresponds to the highest possible scattering angle (180 degree, *i.e.* back-scattering) and can be used to estimate the longitudinal sound velocity c_L:[28]

$$c_L = \frac{\Omega_L \lambda}{2n}, \quad (7)$$

where n is the refractive index of the medium, and λ is the incident wavelength. Fit of the Brillouin spectra (Fig. 2) provides an estimate of the longitudinal sound velocity in the samples.

The temperature dependence of the longitudinal sound velocities obtained for the dry and hydrated samples of all proteins studied are presented in Fig. 4a and b. The values obtained for the longitudinal sound velocity of the proteins are in good agreement with the recent Brillouin neutron scattering data by Paciaroni *et al.*,[29] collected on a perdeuterated dry sample of maltose binding protein (α/β-protein) at room temperature. These studies revealed a high-energy mode that propagates over tens of angstroms with a speed of 3780 ± 130 m s^{-1}, becoming over-damped for Q values greater than 0.8 Å^{-1}. Additionally, quasilongitudinal sound velocities were measured for hydrated tetragonal hen egg-white lysozyme crystals at room temperature using Brillouin light scattering spectroscopy by Speziale *et al.*[27] The measured sound velocities range between 2120 ± 30 m s^{-1} along the [001] direction and 2310 ± 80 m s^{-1} along the [110] direction, in good agreement with our findings for hydrated proteins. Using the sound velocity data we estimated the Young's modulus, E, assuming elastic isotropy, as in Tachibana *et al.*,[30] and applying the relation:[31]

$$E = \frac{(1+\sigma)(1-2\sigma)M_L}{(1-\sigma)}, \quad (8)$$

where σ is Poisson's ratio and M_L is the longitudinal modulus:

$$M_L = \rho {c_L}^2, \quad (9)$$

where ρ is the density of the system. Using density data reported in the literature for the crystalline forms of our proteins (Table S2†), and assuming Poisson's ratio $\sigma \sim 0.33$ (ref. 27) (Table S3†), we calculated the isotropic Young's moduli as a function of temperature and hydration (Fig. 4c and d).

Neutron and light scattering spectra also provide information about vibrational spectra and fast conformational fluctuations (Fig. 3). The latter appear as a broadening of the elastic line known as quasielastic scattering, QES (Fig. 3b and c). The fit of the spectra provided estimates of the boson peak frequency, allowing us to analyse its hydration and temperature dependence (Fig. 5). The frequency of the boson peak decreases with temperature in all proteins, but the effect is more pronounced in hydrated biomolecules. This reflects a softening of the protein with increasing temperature and hydration.

The results of the analysis of the Brillouin data (Fig. 4) reveal a connection of protein rigidity to its secondary structure. Proteins containing α-helices (BSA, MYO) are softer than the protein composed of the β-sheet motif (GFP), and the protein containing both α- and β-structures (lysozyme) shows intermediate rigidity. Dry proteins have a Young's Modulus ranging from ~7 GPa (MYO) to ~13 GPa (GFP) which softens slightly with temperature. Hydrated protein powders are more rigid than dry samples at lower temperature and have the same relationship between the protein secondary structure and rigidity. However, they soften significantly with increases of temperature above ~170–200 K, and become softer than dry samples at room temperature. It is interesting that the largest protein, BSA, shows significantly less variation between dry and hydrated states and with temperature. In the hydrated state, at temperatures over 250 K BSA even appears to have higher sound velocity than would be anticipated from the trend of the other proteins. It is not obvious whether the size of BSA plays any role in this deviation, as a comparison of the ratio of hydrophilic to hydrophobic residues and exposure to water for BSA is similar to those of the other proteins. Analysis of literature data on a broader set of biomolecules is consistent with the observed correlations between the protein secondary structures and rigidity (see Table S4† that includes literature data for different proteins).

The QES intensity of neutron and light scattering spectra represents the amplitude of fast picosecond fluctuations occurring in the proteins.[32,33] The spectra in Fig. 3b and c clearly show that dry samples have a stronger quasielastic contribution at 170 K than the hydrated samples. Yet at 295 K the trend is reversed with the hydrated proteins having a higher QES

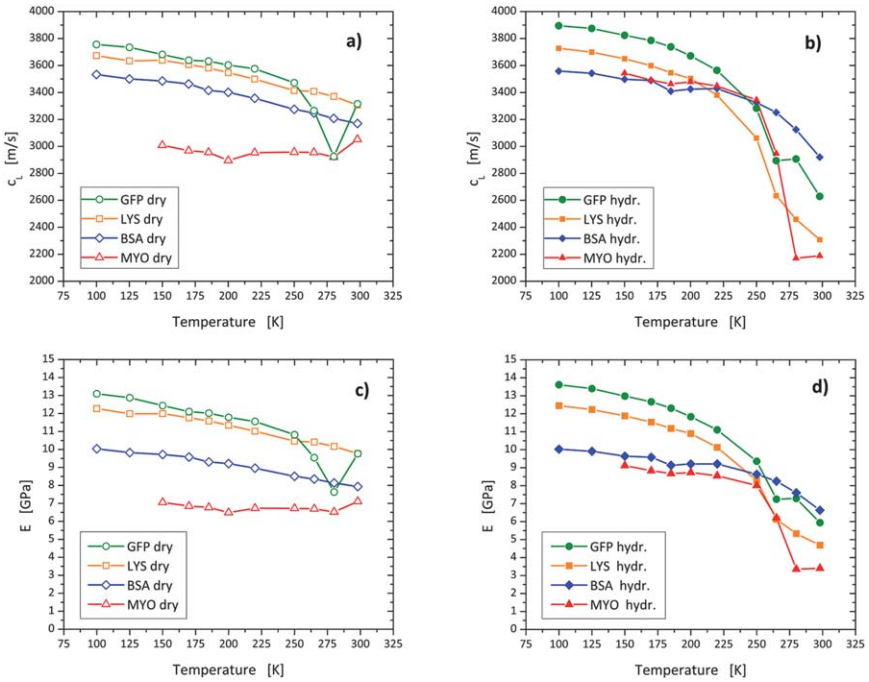

Fig. 4 Longitudinal sound velocity (c_L) as a function of temperature for (a) dry and (b) hydrated samples from Brillouin measurements. Young's modulus data calculated for dry (c) and hydrated (d) proteins using the parameters in Table S2† and assuming Poisson's ratio = 0.33.

intensity than the dry samples. This is in agreement with many earlier studies,[22,33–35] and is explained by the strong interactions with hydration water that suppress dynamics of biomolecules at low temperature, while plasticizing the dynamics at higher temperatures. This low/high temperature picture of relative rigidity between dry and hydrated proteins is consistent with our results for longitudinal sound velocity and elastic modulus. This result is also in agreement with the temperature dependence of the atomic mean squared displacements obtained independently by neutron scattering experiments in GFP.[22]

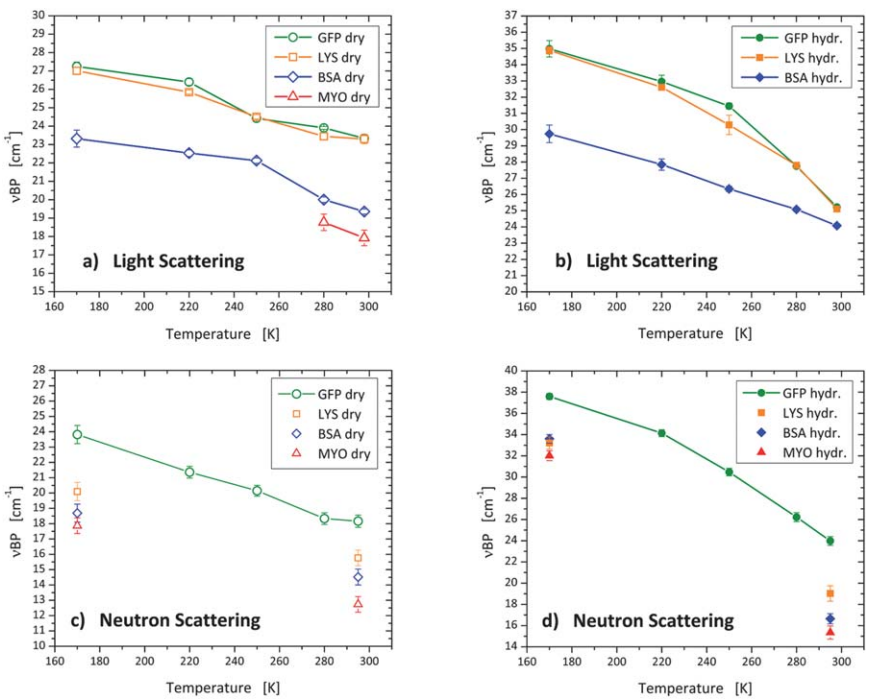

Fig. 5 Boson peak frequencies obtained for all the dry (left panels) and hydrated (right panels) samples from light (a and b) and neutron scattering (c and d) experiments. The error bars are the uncertainties provided by the fit.

In the context of this work, it is interesting that the quasielastic intensity in the studied proteins shows a consistent trend with respect to their secondary structures: the spectra of β-protein GFP shows the weakest QES, as well as the smallest mean squared displacements on a ~30 ps timescale, as measured by neutron scattering (inset in Fig. 1), while the spectra of α-proteins MYO and BSA exhibit significantly higher QES (Fig. 3b and c). This difference persists in both the dry and hydrated states, and at low and high temperatures. Lysozyme has relatively high QES, comparable to that of α-proteins, especially in the hydrated state. This is consistent with Diehl *et al.* who presented neutron spectra of dry lysozyme and myoglobin samples.[33] They concluded that the high QES intensity of lysozyme is related to the high fraction of loop regions in the molecule, which might have larger amplitudes of motion especially in the hydrated state.

Our observations on these four model proteins suggest the possibility that secondary structure not only controls overall rigidity, but also influences the amplitude of fast conformational fluctuations in proteins. In fact, previous neutron data obtained by Gaspar *et al.* for proteins in aqueous solutions[36] appear to be consistent with our findings. They showed that a model β-sheet structure was more rigid and showed smaller quasielastic intensity relative to α-helices on the tens of picoseconds timescale. It seems, however, that the loop regions might contribute significantly to the QES intensity. The microscopic reason for the higher rigidity of the β-structure is not obvious, but it might be related to the higher number of hydrogen bonds per residue in the GFP β-barrel in comparison to the α-helices in MYO and BSA (see Table S5 in the ESI†).

It should be noted that analysis of rigidity on slower, nanosecond timescales might be more complicated. The contribution of motions independent of rigidity, such as methyl group rotations, dominate the spectra at these times.[37] MD simulations suggest that only a fraction of the dynamics in this timescale show a sensitivity to rigidity[38] and the exclusive analysis of elastic neutron scattering data can produce different results.[39]

In contrast to the Brillouin light scattering, which detects propagating sound waves with wavelengths in the order of ~100 nm and frequencies of ~10 GHz,[27] the boson peak vibrational modes are on the sub-picosecond time scale and localized to a region of a few nm. The boson peak is therefore thought to provide information about local elasticity on a smaller length scale. It is a characteristic feature in neutron and light scattering spectra of glass-forming systems. In this case the frequency, ν_{BP}, is usually ascribed to a characteristic size of elastic constant fluctuations $\xi \sim 2$–3.5 nm,[40] or to soft potentials[41] in the disordered structure. A similar peak has been found in both Raman and neutron scattering spectra of all protein powders, in both dry and hydrated states, at a frequency of ~16–32 cm^{-1}.[33–35] The microscopic nature of the boson peak vibrations in proteins remains unknown, although it is thought that these modes might play a crucial role in the function of biomolecules due to the large amplitude of atomic displacements caused by the low-frequency vibrations.

What is known for proteins is that the collective harmonic vibrations associated with the boson peak are distributed through the whole protein;[34,35] and that the backbone, polar and non-polar side-chains all participate.[35] Moreover, these vibrations are strongly coupled to the low frequency motions of hydration water.[35,42] Yet, it is unclear from the literature if the atoms in the entire protein are moving coherently in these modes; or if the boson peak comes from modes involving displacements of groups of atoms, individual amino acid residues, secondary structures, and/or domains.[43]

We now consider our experimental results in the context of several models previously proposed to explain the origin of the boson peak. In our analysis we will use the elastic modulus estimated using Brillouin scattering data, although elastic behaviour at the microscopic and nanoscopic (protein) length scale might differ. The Elastic Global Model[44] connects ν_{BP} to the inverse of the radius of the protein, R, according to the formula

$$\tilde{\nu} = \frac{1}{2cR}\sqrt{\frac{E}{\rho}}, \tag{10}$$

where c is the speed of light in a vacuum, E is Young's modulus, and ρ is the mass density.

The data from both light and neutron scattering clearly shows that the frequency of the boson peak is not related to the size of the protein: BSA and MYO have very similar ν_{BP}, although their diameters differ by more than 1.5 times. This result contradicts the earlier ideas of the Elastic Global Model.[44] The boson peak frequency, however, again exhibits the same trend with respect to the secondary structure of the proteins (Fig. 5): the two α-proteins MYO and BSA have the lowest ν_{BP}, while the β-protein GFP has the highest ν_{BP}, and lysozyme with α- and β-structures is in between. This trend is visible in both sets of NS and LS data; in the LS case, differences in ν_{BP} between the proteins in the hydrated state are less pronounced relative to the neutron data. This can be related to the fact that light scattering intensities depend not only on the vibrational density of the states but also on the light-to-vibration coupling coefficient, and are also affected by background fluorescence. Moreover, in hydrated proteins NS data for ν_{BP} are more relevant due to the relatively low contributions of D_2O. Our result suggests that the boson peak frequency in proteins is sensitive to secondary structure and raises the possibility that the origin of this feature includes modes based on secondary structure elements. Such an explanation is supported by previous literature, such as Brown *et al.*,[45] who showed that the boson peak was connected to the coherent vibrations of adjacent, strongly coupled residues.

It is then logical to consider the model for the low frequency vibrations of polymers, the so-called longitudinal acoustic modes.[46,48,49] The low-frequency Raman peak was assigned to the symmetric, longitudinal, accordion-like motions of the extended zig-zag carbon backbone. In this way a polymer molecule can be approximated by a continuous elastic rod, whose frequency is inversely proportional to the length of the chain, L, according to the equation[46]

$$\tilde{\nu} = \frac{1}{2cL}\sqrt{\frac{E}{\rho}}. \tag{11}$$

In another approach, Chou, working with the Raman spectra of proteins, considered the secondary structure as a relevant

parameter and suggested that the low frequency motions are related to the internal deformation of secondary structures, such as the accordion-like modes of α-helices[50] and β-sheets,[51] and breathing motions of β-barrels.[51] Specifically, by approximating the α-helix to a spring of length L, Chou predicts a frequency of

$$\tilde{\nu} = \frac{1}{2\pi c}\sqrt{\frac{k + K^*}{\rho L/3}} \quad (12)$$

where ρ is the mass per unit length of the spring, K^* is the bending force constant and k depends on the number of residues in the α-helix and on the stretching force constant.[52]

For the β sheet case, the same author considers a vibration system consisting of strands of mass M, and springs (hydrogen bonds, HBs) whose mass is negligible. The obtained accordion-like vibration occurs at frequency

$$\tilde{\nu} = \frac{1}{\pi c}\sqrt{\frac{3\lambda k}{\mu(\mu+1)M}}. \quad (13)$$

λ is the number of HBs (= n + 1, where n is the number of residues in each chain), μ is the number of constituent chains, and k is the stretching force constant of a hydrogen bond.[50]

Finally, by connecting the edges of the strands and springs model of the β-sheet, Chou derived a model for the β barrel, whose breathing motion has a characteristic frequency given by

$$\tilde{\nu} = \frac{1}{\pi c}\left(\sin\frac{\pi}{\mu}\right)\sqrt{\frac{\lambda k}{M}} \quad (14)$$

where μ represents the number of rods, M is the total mass, λ the number of HBs and k is the stretching force constant of a hydrogen bond.[51]

Table 2 compares the ν_{BP} results obtained from the analysis of neutron and light scattering spectra to the frequencies predicted from the continuous elastic rod model and Chou's models. The models were applied to each secondary structural component (α-helix or β-sheet) of the proteins. The length of α-helices was defined as the distance from the first to the final α carbon in each helical unit (using structures from PDB). The averaged values for each protein are presented in Table 3. Values of ν_{BP} calculated from the continuous elastic rod model (eqn (11)) agree well with the light scattering data for MYO and BSA, while deviating strongly for LYS which has short α-helices and β-sheets, and a significant amount of loop regions (Table 1). So, it is possible that this model gives good estimates for the frequency of Raman modes for proteins with strongly dominating secondary structures. Chou's models for accordion-like motions of α-helices and of β-sheets[50-52] are systematically larger for MYO and BSA and a strong difference appears for LYS (Table 2). We want to emphasize that lysozyme is characterized by a substantial loops portion which is not taken into account by these models. It is worth mentioning that these models were optimized for light scattering on long helices/chains,[40,49] and no correction for the light-to-vibration coupling coefficient[53] was performed. On the other hand, Chou's prediction for the breathing mode of GFP, a β-barrel with 109 HBs,[54] gives a ν_{BP} ~17 cm^{-1}, which agrees with the neutron scattering data. So, while Chou offers a reasonable interpretation of ν_{BP} in a β-barrel, the model of accordion-like motions for α-helices is not supported by our data. Chou correctly recognized that the model does not take into account the effects of the immediate surroundings of a given structure. In the case of the β-barrel the surrounding environment would be less of a factor. This might be the reason for the good agreement of the model's prediction and the observed boson peak frequency for GFP (Table 2).

Finally we test the non-continuous model proposed by Duval *et al.*[40,55] to interpret the boson peak of the glass-forming systems. In this model the glass is described as a network disrupted by disordered defects. The boson peak arises from vibrations localized in these nano-heterogeneities that compose the glass. It follows then that the low-frequency vibrational spectra will carry information about the characteristic size and relative stiffness of these local heterogeneities. By combining observations of the boson peak and sound velocity measurements it is possible to estimate the characteristic correlation length scale ξ assuming an acoustic-like nature of the boson peak vibrations according to:[40,55]

$$\xi = s\frac{c_T}{\nu_{BP}}, \quad (15)$$

where ν_{BP} is the boson peak frequency, c_T is the transverse sound velocity, and S is a constant that depends on the particular mode. Assuming a Poisson's ratio of $\sigma = 0.33$ (see Table S3†) gives an estimate of $c_T = c_L/1.98$. For a spherical particle the parameter S for the lowest frequency mode is $s = 0.8$.[40,55]

Table 3 lists the room temperature values of ξ together with the molecular weights and the hydrodynamic radii of the proteins, the average length of the α-helices, and the diameter of the β-barrel. The ξ values estimated using eqn (15) are smaller than the average distance from surface to surface for all the samples investigated. The resulting characteristic lengths for the protein boson peak are therefore reasonable in the context

Table 2 Boson peak frequencies: observed at room temperature for dry proteins with neutron (NS) and light scattering (LS), and calculated for the continuous elastic rod and Chou's models. Error of the fit reported

	ν_{BP} obs. NS (cm^{-1})	ν_{BP} obs. LS (cm^{-1})	ν_{BP} continuous elastic rod model (cm^{-1})	ν_{BP} Chou's models (cm^{-1})
GFP	18 ± 1.0	23 ± 0.5		17
LYS	16 ± 1.0	23 ± 0.5	α-Helices 37	α-Helices 30 β-Sheets 47
BSA	14.5 ± 1.0	19.5 ± 0.5	20	24
MYO	12.5 ± 1.5	18 ± 0.5	20	23

Table 3 Values of the correlation length scale ξ listed together with the molecular weight (M_w), hydrodynamic radius (R_H), average length of the α-helices of the molecules and the average diameter of the β-barrel. The last two parameters have been obtained from the pdb files of the molecules

	M_w (kDa)	R_H (nm)	ξ dry 298 K (nm)	Average length of α-helices (nm)	Average diameter of β-barrel (nm)
GFP	25.8	2.48[46]	1.91	—	2.4 (ref. 47)
LYS	14.3	2.05[45]	1.91	1.23	—
BSA	62.6	3.4[44]	2.20	2.14	—
MYO	17.8	2.12[45]	2.29	2.05	—

of this model. Moreover, our results again confirm that ξ doesn't scale with the molecular weight; it is about two times smaller than the size of the protein. However, the correlation length obtained for BSA and MYO is very close to the average length of the α-helix. The α-helices of lysozyme (1.23 nm) are shorter than those of BSA and myoglobin but the presence of the β-sheets and substantial contribution from loops complicates the picture and a combined contribution of all the structural units has to be expected. The estimated characteristic length scale for GFP does appear close to the diameter of the β-barrel (Table 3). Further studies would be appropriate to unravel the elementary vibrating units for proteins containing β-structures as well as loop and disordered regions. We also note that the boson peak in proteins is very broad (Fig. 3) reflecting the broad distribution of possible modes and length scales.

Although the entire presented study is based on powder samples, we expect that the results obtained for the boson peak in hydrated proteins might be extended to solutions.[56,57] The hydration level $h = 0.4$ is usually considered to be sufficient for full development of protein activity and dynamics.[32,58] Thus the conclusions formulated for hydrated proteins might be relevant when considering proteins in solution.

Conclusions

While it is important to acknowledge that this work has focused on only four model proteins, the presented study reveals a potential connection between secondary structure, rigidity and dynamics in proteins. From Brillouin scattering we see that the studied α-proteins have lower elastic moduli than those dominated by the β motif. This trend is also observed in the frequency of the boson peak, and in the quasielastic neutron scattering intensity, which are sensitive to molecular rigidity. It is visually summarized in Fig. 1 which illustrates the increase in stiffness going from the α-protein myoglobin to the β-structured GFP. The high rigidity of the β-barrel GFP system is also consistent with the estimates of atomic mean square displacements estimated from neutron scattering (inset of Fig. 1). A microscopic reason for higher rigidity of beta structures is not clear, but it might be related to the higher number of H-bonds per residue. Our analysis also presents evidence related to the microscopic origin of the boson peak vibrations in proteins. We have excluded the molecular size dependence of the boson peak by comparing two α-proteins of substantially different molecular weight. Instead, we reveal a possible relationship of the boson peak frequency and the sizes of secondary structures. Results for lysozyme, however, suggest that disordered loop regions play an important role in the dynamics and complicate analysis of the role of secondary structures.

Acknowledgements

This work was supported by DOE through the EPSCoR program (grant DE-FG02-08ER46528) and by the Scientific User Facilities Division, Basic Energy Sciences, U. S. DOE. HO'N and QZ acknowledge the support of the Center for Structural Molecular Biology (Project ERKP291) funded by the Office of Biological and Environmental Research U. S. Department of Energy. Oak Ridge National Laboratory facilities are managed by UT-Battelle, LLC for the U.S. Department of Energy under contract no. DEAC05-00OR22725.

Notes and references

1 M. J. Buehler, *Proc. Natl. Acad. Sci. U. S. A.*, 2006, **103**, 12285–12290.
2 T. Ackbarow, X. Chen, S. Keten and M. J. Buehler, *Proc. Natl. Acad. Sci. U. S. A.*, 2007, **104**, 16410–16415.
3 M. Buehler and S. Keten, *Nano Res.*, 2008, **1**, 63–71.
4 M. Sällman Almén, K. J. V. Nordström, R. Fredriksson and H. B Schiöth, *BMC Biol.*, 2009, **7**, 50.
5 Y. S. Ho, L. M. Burden and J. H. Hurley, *EMBO J.*, 2000, **19**, 5288–5299.
6 M. A. Lemmon, H. R. Treutlein, P. D. Adams, A. T. Brunger and D. M. Engelman, *Nat. Struct. Biol.*, 1994, **1**, 157–163.
7 T. P. Knowles and M. J. Buehler, *Nat. Nanotechnol.*, 2011, **6**, 469–479.
8 M. J. Buehler and Y. C. Yung, *Nature Mater.*, 2009, **8**, 175–188.
9 Z. Shao and F. Vollrath, *Nature*, 2002, **418**, 741.
10 A. V. Kajava and A. C. Steven, *Adv. Protein Chem.*, 2006, **73**, 55–96.
11 S. Keten, Z. Xu, B. Ihle and M. J. Buehler, *Nat. Mater.*, 2010, **9**, 359–367.
12 A. Nova, S. Keten, N. M. Pugno, A. Redaelli and M. J. Buehler, *Nano Lett.*, 2010, **10**, 2626–2634.
13 J. F. Smith, T. P. Knowles, C. M. Dobson, C. E. Macphee and M. E. Welland, *Proc. Natl. Acad. Sci. U. S. A.*, 2006, **103**, 15806–15811.
14 Z. Xu and M. J. Buehler, *Phys. Rev. E: Stat., Nonlinear, Soft Matter Phys.*, 2010, **81**, 061910.

15 T. E. Fisher, A. F. Oberhauser, M. Carrion-Vazquez, P. E. Marszalek and J. M. Fernandez, *Trends Biochem. Sci.*, 1999, **24**, 379–384.
16 T. P. Knowles, A. W. Fitzpatrick, S. Meehan, H. R. Mott, M. Vendruscolo, C. M. Dobson and M. E. Welland, *Science*, 2007, **318**, 1900–1903.
17 S. Keten and M. J. Buehler, *Nano Lett.*, 2008, **8**, 743–748.
18 T. Ackbarow, X. Chen, S. Keten and M. J. Buehler, *Proc. Natl. Acad. Sci. U. S. A.*, 2007, **104**, 16410–16415.
19 G. Luo, Q. Zhang, A. R. D. Castillo, V. Urban and H. O'Neill, *ACS Appl. Mater. Interfaces*, 2009, **1**, 2262–2268.
20 S. Khodadadi, A. Malkovskiy, A. Kisliuk and A. P. Sokolov, *Biochim. Biophys. Acta*, 2010, **1804**, 15–19.
21 G. Ehlers, A. A. Podlesnyak, J. L. Niedziela, E. B. Iverson and P. E. Sokol, *Rev. Sci. Instrum.*, 2011, **82**, 085108.
22 J. D. Nickels, H. O'Neill, L. Hong, M. Tyagi, G. Ehlers, K. L. Weiss, Q. Zhang, Z. Yi, E. Mamontov, J. C. Smith and A. P. Sokolov, *Biophys. J.*, 2012, **103**, 1566–1575.
23 M. Bée, *Quasielastic neutron scattering: principles and applications in solid state chemistry, biology, and materials science*, Adam Hilger, Bristol, England, Philadelphia, 1988.
24 O. F. Nielsen, *Annu. Rep. Prog. Chem., Sect. C: Phys. Chem.*, 1993, **90**, 3–44.
25 R. T. Azuah, Y. Qiu, P. L. W. Tregenna-Piggott, C. M. Brown, J. R. D. Copley and R. M. Dimeo, *J. Res. Natl. Inst. Stand. Technol.*, 2009, **114**, 341–358.
26 C.-s. Zha, T. S. Duffy, H.-k. Mao and R. J. Hemley, *Phys. Rev. B: Condens. Matter Mater. Phys.*, 1993, **48**, 9246–9255.
27 S. Speziale, F. Jiang, C. L. Caylor, S. Kriminski, C. S. Zha, R. E. Thorne and T. S. Duffy, *Biophys. J.*, 2003, **85**, 3202–3213.
28 J. Hernandez, G. Li, H. Z. Cummins, R. H. Callender and R. M. Pick, *J. Opt. Soc. Am. B*, 1996, **13**, 1130–1134.
29 A. Paciaroni, A. Orecchini, M. Haertlein, M. Moulin, V. Conti Nibali, A. De Francesco, C. Petrillo and F. Sacchetti, *J. Phys. Chem. B*, 2012, **116**, 3861–3865.
30 M. Tachibana, K. Kojima, R. Ikuyama, Y. Kobayashi and M. Ataka, *Chem. Phys. Lett.*, 2000, **332**, 259–264.
31 B. A. Auld, *Acoustic fields and waves in solids*, Wiley, New York, 1973, p. 32.
32 J. H. Roh, J. E. Curtis, S. Azzam, V. N. Novikov, I. Peral, Z. Chowdhuri, R. B. Gregory and A. P. Sokolov, *Biophys. J.*, 2006, **91**, 2573–2588.
33 M. Diehl, W. Doster, W. Petry and H. Schober, *Biophys. J.*, 1997, **73**, 2726–2732.
34 V. Kurkal-Siebert and J. C. Smith, *J. Am. Chem. Soc.*, 2006, **128**, 2356–2364.
35 M. Tarek and D. J. Tobias, *J. Chem. Phys.*, 2001, **115**, 1607–1612.
36 A. M. Gaspar, M. S. Appavou, S. Busch, T. Unruh and W. Doster, *Eur. Biophys. J.*, 2008, **37**, 573–582.
37 G. Schirò, C. Caronna, F. Natali and A. Cupane, *J. Am. Chem. Soc.*, 2010, **132**, 1371–1376.
38 L. Hong, D. C. Glass, J. D. Nickels, S. Perticaroli, Z. Yi, M. Tyagi, H. O'Neill, Q. Zhang, A. P. Sokolov and J. C. Smith, *Phys. Rev. Lett.*, 2013, **110**, 028104.
39 M. T. F. Telling, L. Clifton, J. Combet, B. Frick, S. Howells and V. G. Sakai, *Soft Matter*, 2012, **8**, 9529–9532.
40 E. Duval, A. Boukenter and T. Achibat, *J. Phys.: Condens. Matter*, 1990, **2**, 10227–10234.
41 D. A. Parshin, *Phys. Rev. B: Condens. Matter Mater. Phys.*, 1994, **49**, 9400–9418.
42 G. Schirò, C. Caronna, F. Natali, M. M. Koza and A. Cupane, *J. Phys. Chem. Lett.*, 2011, **2**, 2275–2279.
43 J. C. Smith, *Q. Rev. Biophys.*, 1991, **24**, 227–291.
44 Y. Suezaki and N. Gö, *Int. J. Pept. Protein Res.*, 1975, **7**, 333–334.
45 K. G. Brown, S. C. Erfurth, E. W. Small and W. L. Peticolas, *Proc. Natl. Acad. Sci. U. S. A.*, 1972, **69**, 1467–1469.
46 S.-i. Mizushima and T. Simanouti, *J. Am. Chem. Soc.*, 1949, **71**, 1320–1324.
47 M. Ormo, A. B. Cubitt, K. Kallio, L. A. Gross, R. Y. Tsien and S. J. Remingtont, *Science*, 1996, **273**, 1392–1395.
48 W. L. Peticolas, G. W. Hibler, J. L. Lippert, A. Peterlin and H. Olf, *Appl. Phys. Lett.*, 1971, **18**, 87–89.
49 R. F. Schaufele and T. Shimanouchi, *J. Chem. Phys.*, 1967, **47**, 3605–3610.
50 K. C. Chou, *Biophys. J.*, 1984, **45**, 881–889.
51 K. C. Chou, *Biophys. J.*, 1985, **48**, 289–297.
52 K. C. Chou, *Biochem. J.*, 1983, **209**, 573–580.
53 A. P. Sokolov, U. Buchenau, W. Steffen, B. Frick and A. Wischnewski, *Phys. Rev. B: Condens. Matter Mater. Phys.*, 1995, **52**, R9815–R9818.
54 V. Helms, T. P. Straatsma and J. A. McCammon, *J. Phys. Chem. B*, 1999, **103**, 3263–3269.
55 A. Boukenter, B. Champagnon, E. Duval, J. Dumas, J. F. Quinson and J. Serughetti, *Phys. Rev. Lett.*, 1986, **57**, 2391–2394.
56 M. Marconi, E. Cornicchi, G. Onori and A. Paciaroni, *Chem. Phys.*, 2008, **345**, 224–229.
57 S. Perticaroli, *et al.*, *J. Phys. Chem. B*, 2010, **114**, 8262–8269.
58 I. D. Kuntz Jr and W. Kauzmann, in *Advances in protein chemistry*, ed. C. B. Anfinsen, J. T. Edsall and F. M. Richards, Academic Press, 1974, vol. 28, pp. 239–345.